Journal of Solid State Chemistry **155,** 129–137 (2000)
doi:10.1006/jssc.2000.8913, available online at http://www.idealibrary.com on IDEAL®

Lattice Oxygen Transfer in Fluorite-Type Oxides Containing Ce, Pr, and/or Tb

Z. C. Kang and L. Eyring

Department of Chemistry and Biochemistry, Arizona State University, Tempe, Arizona 85287-1604

Received June 8, 2000; accepted August 2, 2000

DEDICATED TO PROFESSOR J. M. HONIG

Oxygen transfer capacity (OTC) is needed, for example, in three-way catalysts (TWC) for treatment of exhaust gases, extraction of pure oxygen from gaseous mixtures such as air, or the extraction of hydrogen from hydrogen-containing compounds such as water or methane. This property is explored in fluorite-related materials of the formula $Ce_{1-x-y-z-p}Pr_xTb_yM_zR_pO_{2-x}$ ($x+y+z>0.5$) in which *M* is a metal, especially Zr, Ti, V, Mo, W, Nb, Mn, Cu, Cr, Fe, Ni, Co, Ta, and Bi, and in which *R* is another rare-earth element. The OTC of these oxides is inherent in the characteristics of fluorite-related structures and the variable valency of Ce, Pr, and/or Tb. Such oxides can have the OTC property under reducing and oxidizing conditions without any reconstructive phase transitions. OTC data of some binary, ternary, and quaternary oxides containing Ce, Pr, or Tb are discussed. © 2000 Academic Press

Key Words: **oxygen transfer capacity (OTC); oxygen storage capacity (OSC); fluorite-related oxides; hydrogen production from water; three-way catalysts (TWC).**

1. INTRODUCTION

The use of gasoline as a fuel in an internal combustion engine results in the emission of carbon monoxide, hydrocarbons, and NO_x. These toxic gases must be removed to reduce air pollution. Three-way catalysts (TWC) in a catalytic converter can simultaneously oxidize all three pollutants to render them relatively harmless. The catalytic converter contains an oxide capable of providing an adequate oxygen transfer capacity (OTC) for use and replenishment of oxygen. A sustained intermittent supply of oxygen without cyclic replacement is impossible.

Although the precious metals (for example Pt and Rh) can perform in this way to some degree, they have inadequate capacity at reasonable cost. Ceria has been found to possess these qualities (1). Now ceria and Ce–Zr oxides are intensively studied as three-way catalyst promoters. To possess an OTC demands that the cations in the oxide be able to access a variable valence under prevailing redox conditions. In this document we urge further consideration of ceria's partners among the higher rare-earth oxides, praseodymium and terbium, and advantageous dopants among the other elements, which form fluorite-related oxide systems of variable composition.

2. RESULTS AND DISCUSSION

2.1. The Relationship between the Oxygen Content of an Oxide, Temperature, and Oxygen Partial Pressure

To measure the capability of an oxide to store oxygen, a temperature-programmed reduction (TPR) procedure is frequently followed and the result is called the oxygen storage capacity (OSC). In this experiment the rate of oxygen release from an oxide is measured as a function of temperature change, $\Delta f(T)/\Delta T$, under flowing hydrogen or carbon monoxide. The released oxygen can be determined by the rate of consumption of hydrogen or carbon monoxide detected from the mass-spectral peak of water or carbon dioxide (2) or by an oxygen pump (3). The data are often plotted as the change in the oxygen content, Δf, against the increasing temperature. If $\Delta f/\Delta T = 0$ the oxide has no OSC. If it is constant with a positive slope the oxide can supply oxygen continuously with rising temperature. If $\Delta f/\Delta T$ is a curve with a maximum, the oxide can provide more oxygen in that temperature range. Figure 1 illustrates these different possibilities.

In the TPR experiment the oxygen partial pressure in the system may be varied and the rate of flow of the hydrogen or carbon monoxide is usually indicated. This experiment focuses attention on the released oxygen from the oxide, but not on the oxide itself. It could have the same meaning if the change of the oxygen content of the oxide were monitored instead. That is, if the relationship between the oxygen content of an oxide, temperature, and oxygen partial pressure is measured the OSC can be quantified by a differential operation on the reaction curve. Figure 2 is an example.

The relationship between the equilibrium oxygen content of CeO_{2-x}, the oxygen partial pressure, and the

0022-4596/00 $35.00

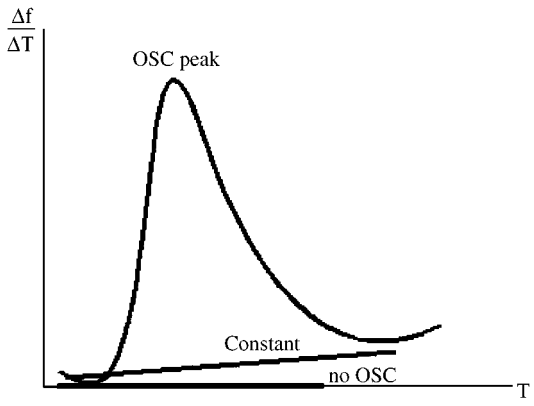

FIG. 1. $\Delta f/\Delta T$ as a function of the temperature, T.

temperature has been published (4). The OSC can be deduced from this data. Figure 2a is the relationship of the equilibrium oxygen content of CeO_{2-x}, oxygen partial pressure, and the temperature. Figure 2b is the OSC of CeO_{2-x} deduced from the evaluation of $\Delta f/\Delta T$ of the curves of 2a at 50°C intervals. Successive peaks mark the temperature range of oxygen release at increasing partial pressures of oxygen. The OSC should be apparent from the original thermodynamic curves themselves.

Figure 3 records the published experimental results that demonstrate the shift of oxygen release from cerium dioxide in the TPR to a higher temperature due to an increased oxygen activity. In the bottom curve 15% H_2 was used to reduce the sample (BET 10 $m^2 g^{-1}$) (1), but in the other only 5% H_2 was used for a sample with a higher surface area (BET 196 $m^2 g^{-1}$) (5). The oxygen partial pressure determines the temperature of oxygen release because the reducibility of an oxide depends on the oxygen activity which itself is temperature dependent. In this paper we will sometimes replace OSC with OTC to make explicit this necessary reversible characteristic for TWC performance. OTC can best be determined from equilibrium data.

2.2. *The Cyclic Availability of the Lattice Oxygen of Higher Order Phases of the Oxides Containing Ce, Pr, and Tb*

2.2.1. Binary oxides. The release or absorption of lattice oxygen frequently accompanies a phase transition. For example, the oxides of titanium, vanadium, and molybdenum release or absorb their lattice oxygen accompanied by changes in the connections between the coordination octahedra formed by titanium, vanadium, or molybdenum with oxygen. This process usually involves a large energy change and leads to a phase transition with distortions and structural modifications that usually are not readily reversible (6).

Rare-earth higher oxides, CeO_{2-x}, PrO_{2-x}, and TbO_{2-x}, on the other hand, have fluorite-related structures

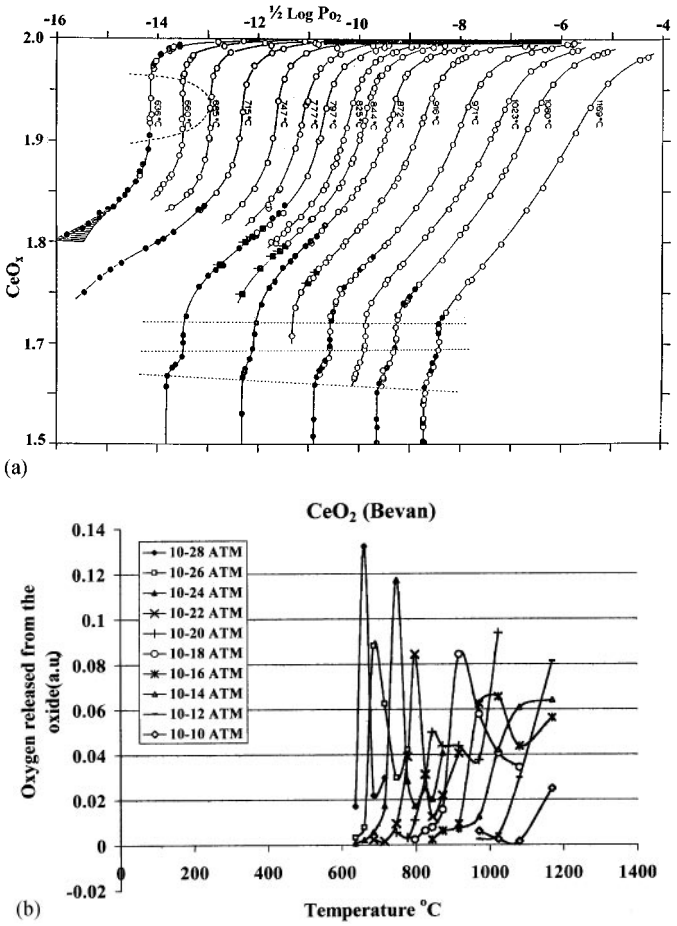

FIG. 2. (a) Relationship between the oxygen content of CeO_{2-x}, oxygen partial pressure, and temperature (adapted from Ref. 4). (b) the OSC of CeO_{2-x} deduced for each oxygen partial pressure studied.

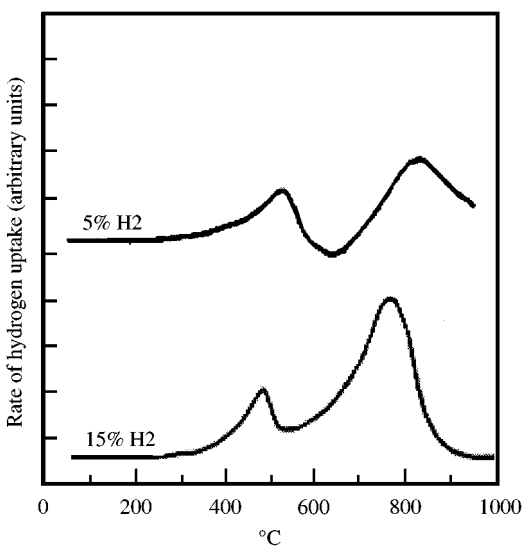

FIG. 3. The peaks of oxygen release from CeO_{2-x} in the TPR process are shifted due to the oxygen partial pressure difference.

in which there is a less directional quality of the bonding. The isothermal (7–9) and isobaric (10–12) data for CeO_{2-x}, PrO_{2-x}, and TbO_{2-x} are available. The phase transition between different intermediate phases occurs without loss of the fluorite sublattice. The oxygen sublattice is independent and the migration of an oxygen ion does not require a substantial cooperative movement of any metal atom. Of course, a slight distortion of the metal and the oxygen atom positions around an oxygen vacancy will occur. These irregularities will be transformed into a distortion wave in the metal sublattice, as an ordered intermediate phase is approached or formed.

An HREM image reveals the types of changes that occur during the oxidation or reduction of these oxides by the change of the modulation contrast. Figure 4 illustrates this phenomenon.

In the image of Fig. 4, the darker bands are the contrast from the distortion modulation of the Pr cations and oxygen atoms around the oxygen vacancies. The Pr sublattice can be seen as a regular array of white dots, especially in the thinner regions. This special structural character gives the rare-earth higher oxides their marked, reversible OTC properties.

Figure 5a illustrates the OTC for PrO_{2-x} for two isobars, one with an increasing temperature and one with a decreasing temperature of 1.5°C min and an equilibrium pressure of 137 Torr oxygen. Readings are taken at 50°C intervals.

The complexities of the PrO_x system is most clearly shown in the heating curve but is also apparent in the cooling curve. Notice particularly the definite shift in these features with temperature, a characteristic that signals hysteresis and other subtle qualities of possible usefulness.

Figures 5b and 5c show the OSC of PrO_{2-x} and TbO_{2-x} at several different partial pressures of oxygen. The complex peaks, due to oxygen release, are observed to shift with the variation in oxygen partial pressure. Because the OSC of PrO_{2-x} and TbO_{2-x} can be seen at higher oxygen partial pressures the hysteresis effect (the release and

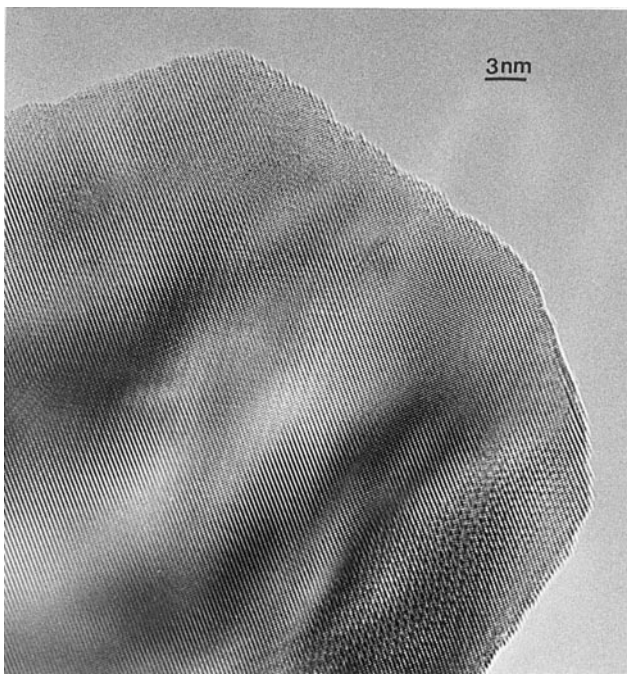

FIG. 4. The modulation contrast indicates the oxygen vacancy configuration in praseodymium oxide, PrO_{2-x}. The modulation contrast will change with the oxygen content and temperature.

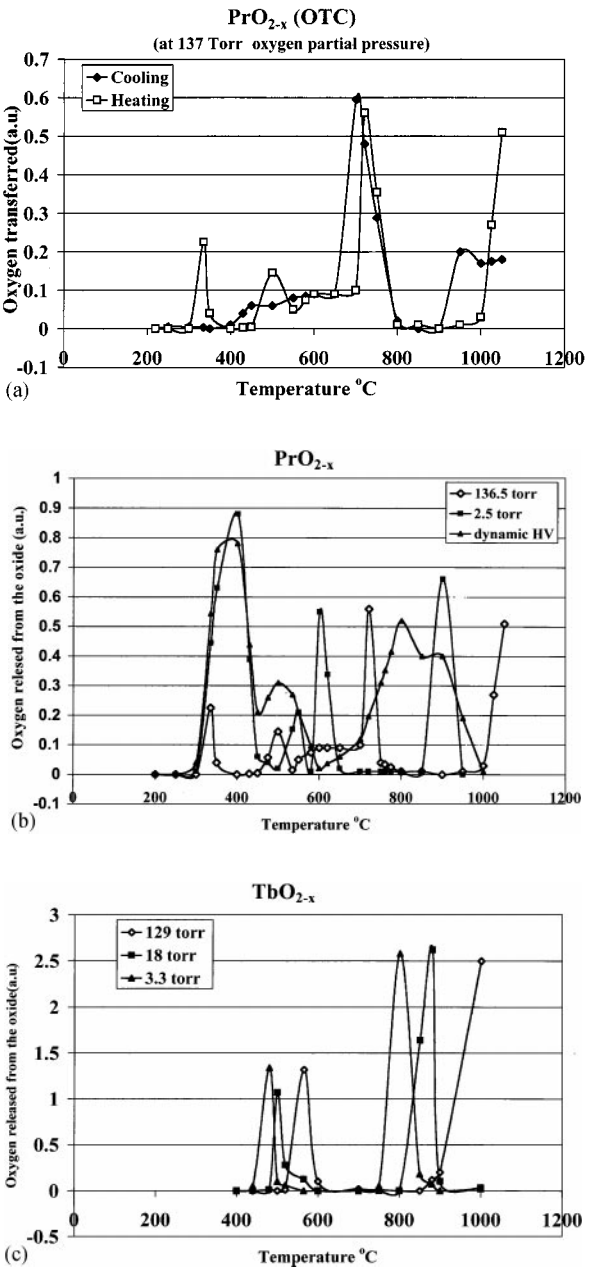

FIG. 5. (a) The OTC of PrO_{2-x} at 137 Torr oxygen. (b) The OSC of PrO_{2-x} and (c) TbO_{2-x}.

absorption of oxygen occurs at different temperatures in oxidation and reduction (7)) will be even more apparent in the OTC.

2.2.2. Ternary oxides. There are two types of ternary oxides containing Ce, Pr, or Tb with fluorite-related structure; one is a solid solution of two of the oxides. The second is an oxide containing only one of the elements, Ce, Pr, and Tb, plus a different metal ion.

The ternary isobaric data of Ce–Tb–O (11) and Pr–Tb–O (13) systems are available. Figure 6 gives the OSC data for the oxides $Ce_{0.9}Tb_{0.1}O_{2-x}$, $Pr_{0.75}Tb_{0.25}O_{2-x}$, $Ce_{0.5}Pr_{0.5}O_{2-x}$, and the OTC of $Ce_{0.5}Pr_{0.5}O_{2-x}$. The peaks of oxygen release are located at different temperatures under different oxygen partial pressures. For the $Ce_{0.9}Tb_{0.1}O_{2-x}$ oxide (Fig. 6a), the peak of oxygen release is higher when the oxygen partial pressure is lower. For example, in these data the highest peak is around 420°C under 2×10^{-4} Torr oxygen. It is apparent from Fig. 2 that 10% Tb in CeO_{2-x}, increases the peak of oxygen release and shifts it to lower temperatures and higher oxygen partial pressures. For the $Pr_{0.75}Tb_{0.25}O_{2-x}$ oxide (Fig. 6b), the first peaks of oxygen release under a different oxygen partial pressure is located at around 360°C. This implies that there is good OSC character at lower temperatures without limiting the oxygen partial pressure. On the other hand, at very low oxygen partial pressure, e.g., flowing hydrogen there is only one peak of significant size at nearly 600°C. In the case of Figs. 6c and 6d (50 mol% Pr in CeO_{2-x}), the available lattice oxygen is provided at lower temperatures. Furthermore, there is almost complete reversibility in reduction and oxidation and no obvious hysteresis. Extensive data for the OTC for different compositions of these fluorite-related oxides have been acquired (14).

Notice that if the reducing condition (or oxygen partial pressure) and the temperature required for supplying lattice oxygen are known, it could be possible to find a doped oxide with Ce and Pr, or Ce and Tb, or Pr and Tb to satisfy the need.

Ce–Zr–O (5) and Ce–Cu–O (15) systems are known to have an OSC. Figure 7 shows the OSC of the oxide $Ce_{0.62}Zr_{0.38}O_{2-x}$.

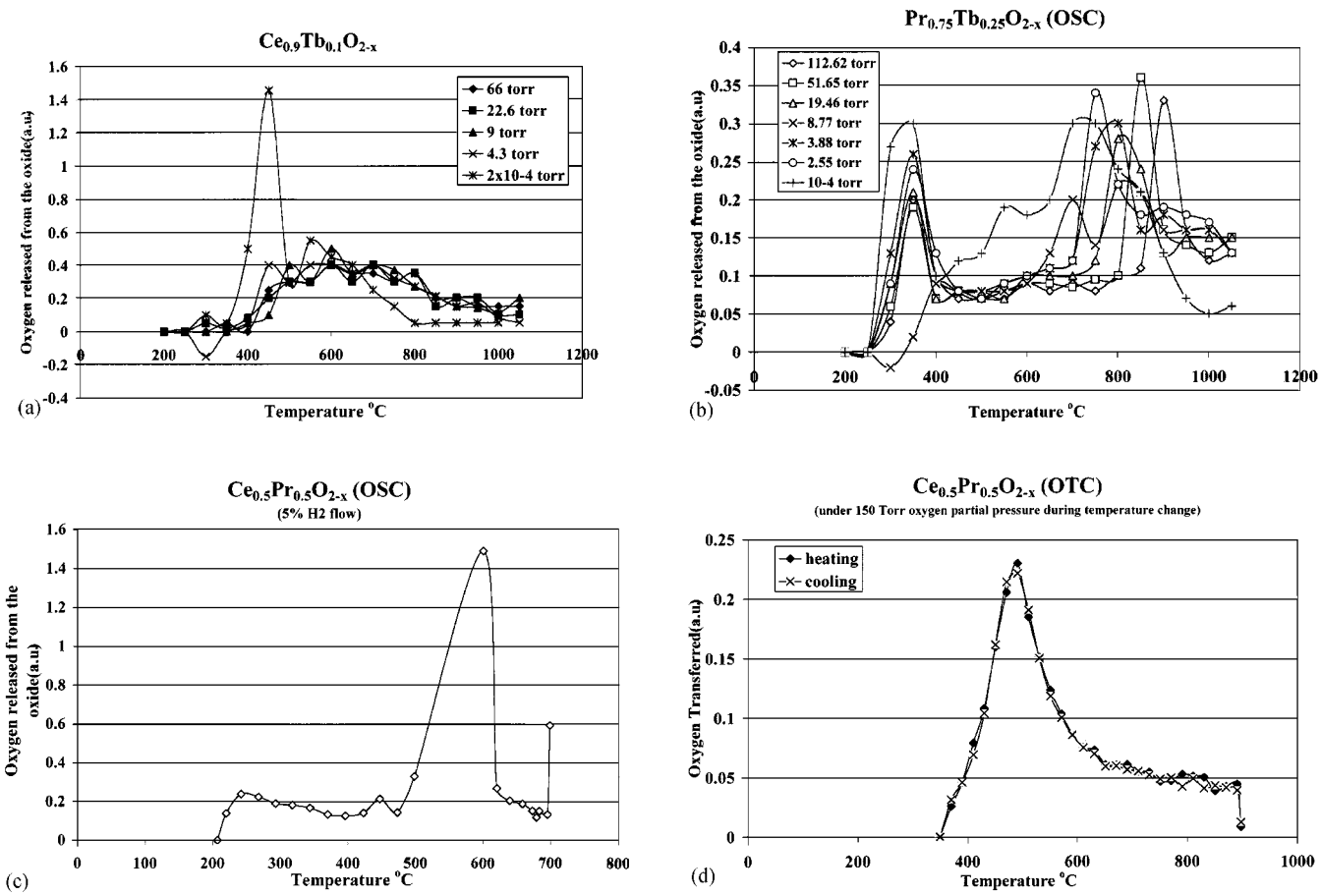

FIG. 6. The OSC of $Ce_{0.9}Tb_{0.1}O_{2-x}$ (a), $Pr_{0.75}Tb_{0.25}O_{2-x}$ (b), and $Ce_{0.5}Pr_{0.5}O_{2-x}$ (c) and also the OTC of $Ce_{0.5}Pr_{0.5}O_{2-x}$ (d) under 150 Torr oxygen pressure.

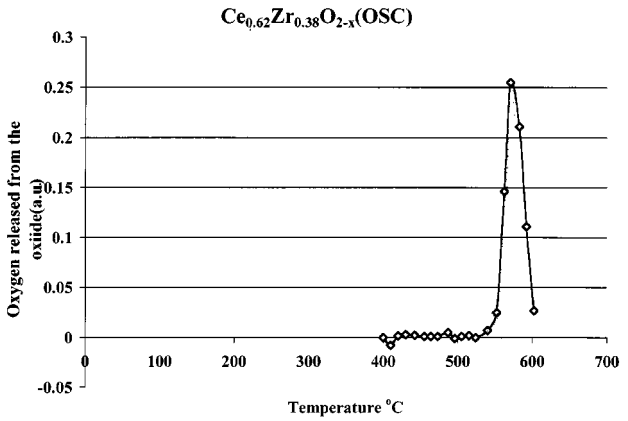

FIG. 7. The OSC of the oxide $Ce_{0.62}Zr_{0.38}O_{2-x}$.

Doping CeO_2 with Zr promotes the lattice oxygen availability. The amount of available lattice oxygen depends on the cerium content. The available lattice oxygen would decrease as the doping is increased. However, doping CeO_2 with Pr or Tb will not only shift the peak to lower temperatures, but will also increase the amount of available lattice oxygen.

2.2.3. Quaternary. Figure 8 shows the OSC data for $Ce_{0.7}Zr_{0.25}Tb_{0.05}O_{2-x}$. In Fig. 8a the oxygen release in flowing 5% H_2 is seen to occur as a broad peak around 500–600°C, but in Fig. 8b the reducing agent is flowing 15% methane and the peak showing oxygen release has shifted to around 700°C. The availability of lattice oxygen for this oxide varies over a very wide temperature range and is still increasing at 900°C. Under a partial pressure of 150 or 3 Torr of oxygen the lattice oxygen release from this oxide is still available as the temperature is increased from 200 to 900°C. $Ce_{0.7}Zr_{0.25}Pr_{0.05}O_{2-x}$ behaves similarly when Pr is substituted for Tb.

If we compare the OSC of $Ce_{0.7}Zr_{0.25}Tb_{0.05}O_{2-x}$ with CeO_{2-x} the oxygen release peak of the former is shifted to lower temperatures and is broader, but also the oxygen partial pressure is much higher than for CeO_2. As the data of the ternary system of Ce, Pr, and Tb indicated, the content of Pr, and/or Tb increases the oxygen release peak and shifts it to lower temperatures and at higher oxygen partial pressures. The OSC property can certainly be improved by doping with other elements, but one must be careful to maintain the fluorite-related structure.

2.3. Oxygen Transfer from Water and Carbon Monoxide

The lattice oxygen released under reduction or high temperature should be reabsorbed if the oxygen partial pressure is increased or the temperature is decreased. Indeed, reduced CeO_{2-x} (16) or $Ce_{0.7}Zr_{0.25}Tb_{0.05}O_{2-x}$ (17) can absorb combined oxygen from water, releasing hydrogen.

Figure 9 shows oxygen absorption from water by $Ce_{0.7}Zr_{0.25}Tb_{0.05}O_{2-x}$ at 573 K which has been reduced by 5% H_2 or by 15% CH_4. There is a difference in these two oxidations from a kinetic point of view. The oxygen absorption of the hydrogen reduced oxide (Fig. 9a) is faster than by the one reduced by methane (Fig. 9b). These reduced oxides can absorb oxygen from many sources, for example H_2O and CO.

The reduction of H_2O does produce hydrogen as demonstrated by the results shown in Fig. 10. The amount of absorbed oxygen is also a function of temperature and water partial pressure. The voltage developed in a fuel cell incorporating a NAFION membrane in series with the exit gas flow, as recorded in Fig. 10, confirms that hydrogen is produced.

These experimental data clearly demonstrate a critical application for the OTC of oxides containing Ce, Pr, and Tb. It is definitely possible to cycle the temperatures of methane and water to continuously produce hydrogen, which in turn can be transformed directly into electrical energy by a fuel cell. The thermal energy needed for heating

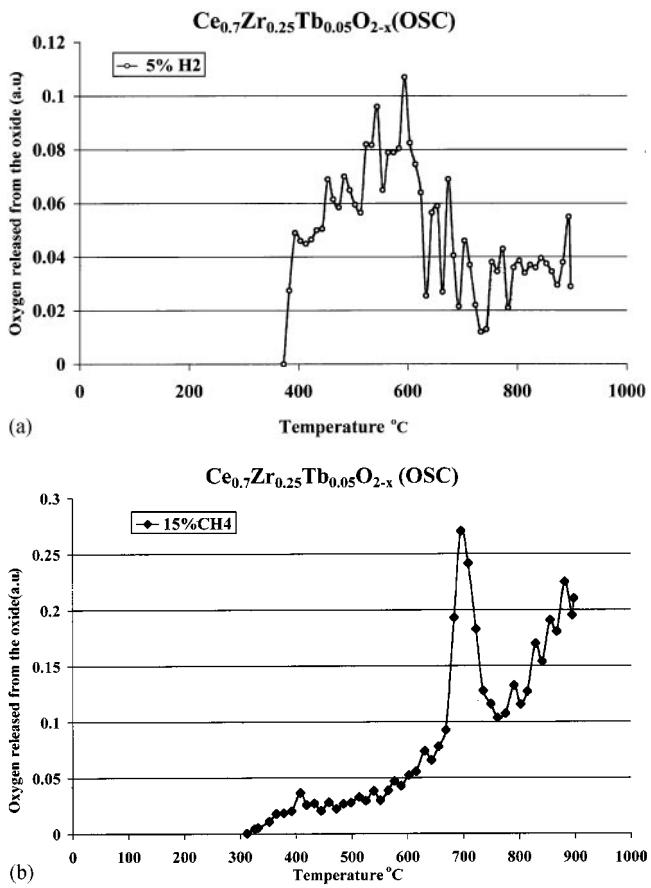

FIG. 8. Oxygen release from the $Ce_{0.7}Zr_{0.25}Tb_{0.05}O_{2-x}$ under (a) flowing 5% H_2 (b) flowing 15% CH_4.

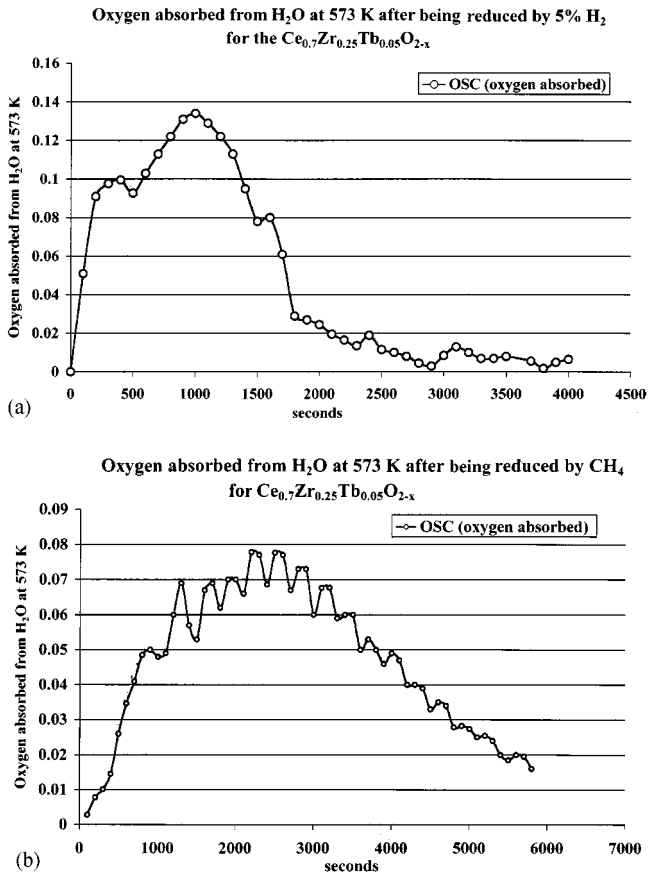

FIG. 9. The oxygen absorption from H_2O vapor by reduced $Ce_{0.7}Zr_{0.25}Tb_{0.05}O_{2-x}$ at 570 K by (a) 5% H_2 and (b) 15% CH_4.

the oxide could be obtained from solar energy which is more than 80% thermal (17).

2.4. An HREM Study of Carbon Oxidation by Oxide Lattice Oxygen

As mentioned before, methane can be oxidized by ceria to hydrogen and carbon monoxide:

$$CeO_2 + xCH_4 \rightarrow CeO_{2-x} + 2xH_2 + xCO.$$

If the CeO_2 has been reduced far enough it may pick up oxygen from the carbon monoxide to form carbon:

$$CeO_{2-x} + \delta CO \rightarrow CeO_{2-x+\delta} + \delta C.$$

The carbon is deposited on the oxide surface to form carbon layers as shown in Fig. 11. The cerium oxide becomes completely black from the carbon deposit as is $Ce_{0.7}Zr_{0.25}Tb_{0.05}O_{2-x}$. These carbon layers do not prevent oxygen absorption from any source, for instance H_2O. It is possible to observe the oxidation of the carbon layer to CO_2

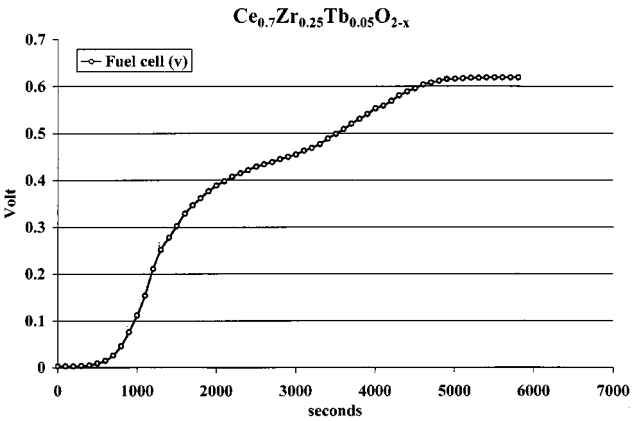

FIG. 10. The voltage of a fuel cell registered by hydrogen release from water.

in the electron microscope due to the oxygen released from the oxide during imaging. Figure 12 shows this process of oxidation of deposited carbon from the $Ce_{0.7}Zr_{0.25}Tb_{0.05}O_{2-x}$ (after methane reduction and carbon deposit). In Fig. 12a the amorphous carbon covers the whole crystal cluster, but after about 20 min (Fig. 12b) the carbon layer has thinned. Modulation contrast simultaneously appears in the crystal (Figs. 12a and 12b). This is interpreted as lattice oxygen released from the oxide oxidizing the carbon. After about 40 min (Fig. 12c) the amorphous carbon layers are almost gone and the surface atoms can be seen distinctly. After 50 min all of the crystals have clean surfaces (Fig. 12d). This observation further confirms the release of lattice oxygen and its reabsorption without reconstruction

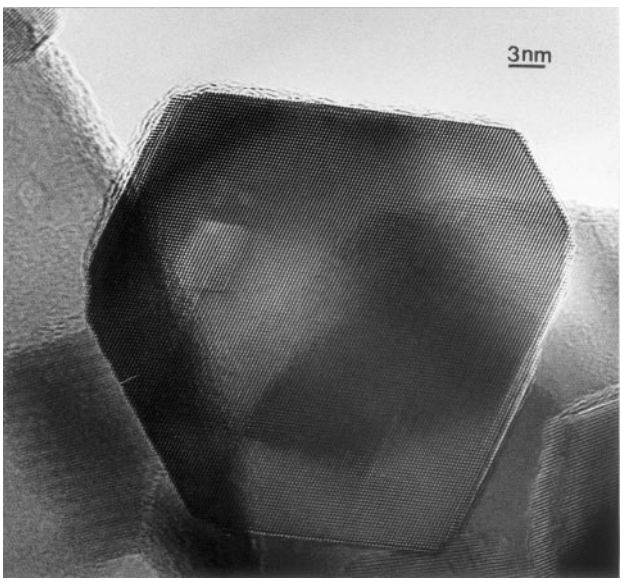

FIG. 11. An amorphous carbon layer deposited on the surface of a CeO_2 crystal due to the reduction of CO.

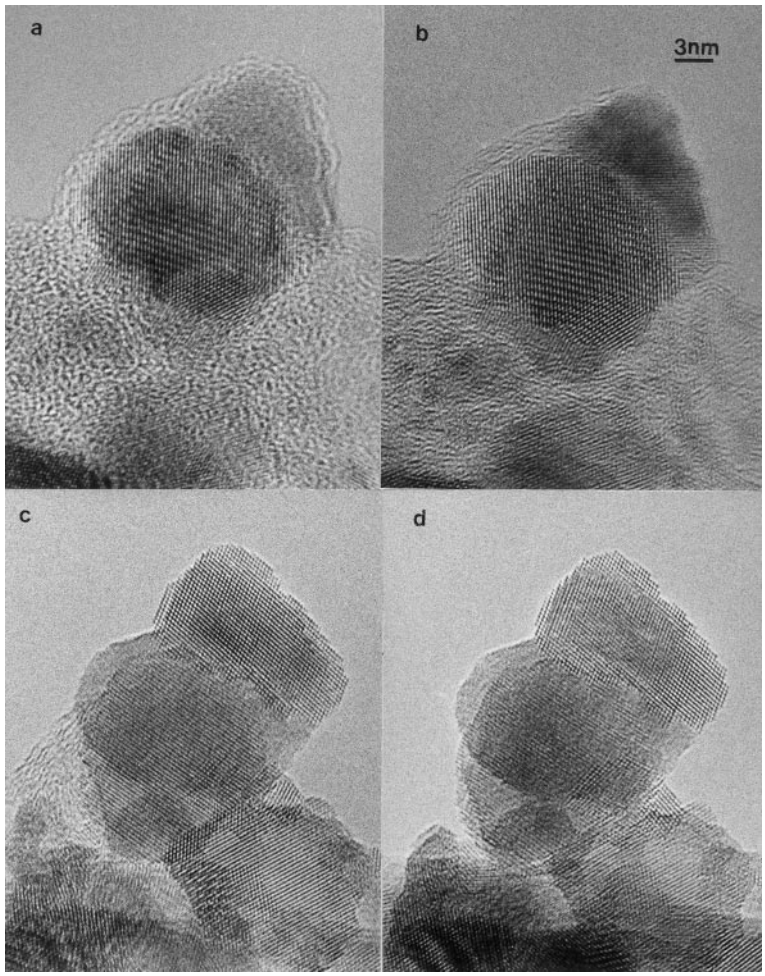

FIG. 12. Deposited carbon oxidized by released oxygen from the $Ce_{0.7}Zr_{0.25}Tb_{0.05}O_{2-x}$ oxide. (a) Deposited carbon on the crystals (b) after 20 min and (c) after 40 min electron beam radiation, and (d) finally after 50 min. The modulation in the crystal seen in (a) and (b) indicates oxygen migration during release of oxygen from the oxide.

of the fluorite lattice. Furthermore, the process reveals the development of distortion modulations due to oxygen vacancy migration during decarbonation.

2.5. Lattice Oxygen Availability from the Fluorite-Related Pyrochlore Structures

As demonstrated, the oxygen sublattice of the fluorite structure is flexible, allowing easy oxygen ion migration. The expansive distortion of the cations around the oxygen vacancies and the adjacent oxygen ions slightly shifting toward the vacancy position makes the activation energy for oxygen migration relatively small (18). The Ce, Pr, or Tb cations can simultaneously vary their valence state by electron hopping to coordinate with the oxygen vacancy migration. If this condition holds, the OTC will be marked.

The pyrochlore structure can be seen as an assemblage of eight fluorite-type modules and eight oxygen vacancies in a cubic array. Therefore, OTC would be expected. Table 1 lists all of the possible compositions and structures of oxides comprising this unit cell.

In Table 1, U or D means a fluorite unit with an oxygen vacancy at the top or bottom layer, respectively, of the oxygen cube in a fluorite unit cell, W is a fluorite unit with two oxygen vacancies across the body-diagonal of the oxygen cube, and F represents a fluorite unit with no oxygen vacancies (19). No superstructure means that the oxygen vacancies cannot form a superstructure under the assigned conditions; in other words it is a fluorite structure with disordered oxygen vacancies. The possible superstructures are pyrochlore, fcc, bcc, and simple cubic. All of them would have unit cell dimensions similar to those of pyrochlore. We may call them all pyrochlore-type structures. The oxygen content of these phases would vary from $A_2B_2O_7$ to $A_2B_2O_8$. They are usually represented as $A_2B_2O_{7+\delta}$ $(0 < \delta < 1)$. If A is Ce, and B is Zr, the composition could

TABLE 1
Possible Fluorite-Related Pyrochlorite-Type Phases

Modules composing the phase	Composition of the phase
8F (fluorite)	$R'''_{32}O_{64} = RO_2$
4U4D (pyrochlorite)	$R'_{16}R''_{16}O_{56} = R'_2R''_2O_7$
4U3DF (no superstructure)	$R'_{16}R''_{12}M_4O_{57} = R_7MO_{14.25}$
3UD2F (no superstructure)	$R'_{12}R''_{12}M_8O_{58} = R_6M_2O_{14.5}$
3U2D3F (no superstructure)	$R'_{12}R''M_{12}O_{59} = R_5M_3O_{14.75}$
2UD4F (no superstucture)	$R'_8R''_8M_{16}O_{60} = R_2M_2O_{7.5}$
4U4F or 4D4F (fcc)	$R'_8R''_8M_{16}O_{60} = R_2M_2O_{7.5}$
WUDU4F (no superstructure)	$R'_8R''_4R'''_4M_{16}O_{59} = R_2M_2O_{7.375}$
2WUD4F (no superstructure)	$R'_4R''_4R'''_8M_{16}O_{58} = R_2M_2O_{7.25}$
3WU4F (no superstructure)	$R'_4R'''_{12}M_{16}O_{57} = R_2M_2O_{7.125}$
4W4F (fcc)	$R'''_{16}M_{16}O_{56} = R_2M_2O_7$
2UD5F (no superstructure)	$R'_8R''_4R'''_4M_{16}O_{61} = R_2M_2O_{7.625}$
2UD5F (no superstructure)	$R'_8R''_4M_{20}O_{61} = R_3M_5O_{15.25}$
WUD5F (no superstructure)	$R'_4R''_4R'''_4M_{20}O_{60} = R_3M_5O_{15}$
WUD5F (no superstructure)	$R'_4R''_4R''_4R'''_4M_{16}O_{60} = R_2M_2O_{7.5}$
2WU5F (no superstructure)	$R'_4R''_8M_{20}O_{59} = R_3M_5O_{14.75}$
2WU5F (no superstructure)	$R'_4R''_8R'''_4M_{16}O_{59} = R_2M_2O_{7.375}$
3W5F (no superstructure)	$R'_{12}M_{20}O_{58} = R_3M_5O_{14.5}$
3W5F (no superstructure)	$R'_{12}R''_4M_{16}O_{58} = R_2M_2O_{7.25}$
UD6F (cubic)	$R'_8R''_8M_{16}O_{62} = R_2M_2O_{7.75}$
WU6F (no superstructure)	$R'_4R''_4M_{24}O_{61} = RM_3O_{7.625}$
WU6F (no superstructure)	$R'_4R''_4R''_8M_{16}O_{61} = R_2M_2O_{7.625}$
WW6F (no superstructure)	$R''_8M_{24}O_{60} = RM_3O_{7.5}$
WW6F (bcc)	$R''_8R''_8M_{16}O_{60} = R_2M_2O_{7.5}$
U7F (cubic)	$R'_4R''_{12}M_{16}O_{63} = R_2M_2O_{7.875}$
W7F (cubic)	$R'_4R''_{12}M_{28}O_{62} = R_2M_2O_{7.75}$
8W	$R''_{32}O_{48} = RO_{1.5}$

vary from $Ce_2Zr_2O_7$ to $Ce_2Zr_2O_8$ depending on the Ce and Zr content. If all of zirconium ions are substituted by cerium, $A_2B_2O_6$ is the cerium sesquioxide and the $A_2B_2O_8$ is cerium dioxide. The cerium content determines the value of the OTC of the oxide. For 50 mol% Ce and 50 mol% Zr system the compositions of the pyrochlore-type phases may be as $Ce_2Zr_2O_7$, $Ce_2Zr_2O_{7.5}$, $Ce_2Zr_2O_{7.75}$, up to $Ce_2Zr_2O_{7.875}$. From a structural point of view the cations of Ce and Zr may be completely disordered or partially ordered. Figure 13 shows an HREM image of a predominantly pyrochlore-type simple cubic phase of $Ce_2Zr_2O_{7.75}$ with two oxygen vacancies in its unit cell. Also included in the image is a small pyrochlore domain in the top right-hand corner (20).

The calculated diffraction pattern from a proposed structure model is given in Fig. 14. The DDPs (digital diffraction patterns (21)) from different areas on the image indicate a small domain with pyrochlore structure located at the top right corner. Figure 15 shows another HREM image of $Ce_{0.5}Zr_{0.5}O_{2-x}$ in which a small pyrochlore domain appears in the fluorite-type crystal in the bottom left-hand corner. It seems that domains of different phases coexisting together are characteristic of this $Ce_{0.5}Zr_{0.5}O_{2-x}$ crystal which was reduced at high temperature, higher than

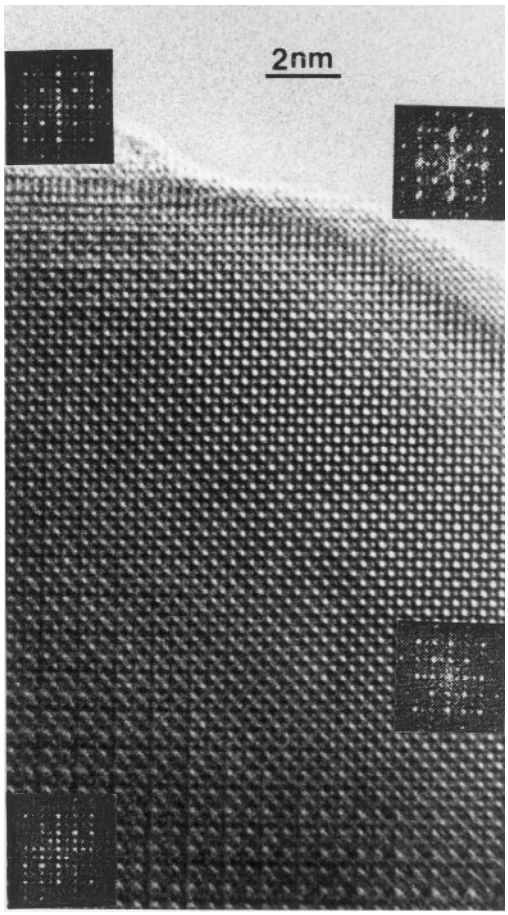

FIG. 13. HREM image of a new phase, $Ce_2Zr_2O_{7.75}$, with a pyrochlore-type domain at the top right corner. The DDP is inserted at this location.

1000°C, and then reoxidized at an intermediate temperature.

3. SUMMARY AND CONCLUSIONS

3.1. Fluorite-Related Oxides Containing Ce, Pr, and Tb with OTC (or OSC) Properties

The compositions of the materials used in experiments discussed here are subsets from the large set of fluorite-related oxides having the formula $Ce_{1-x-y-z-p}Pr_xTb_y$

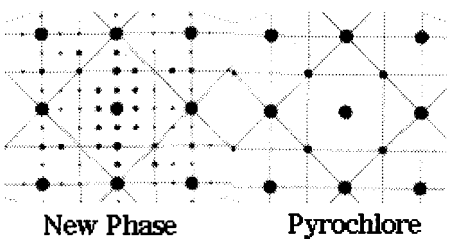

FIG. 14. Calculated diffraction pattern from a simple cubic model with two oxygen vacancies and the pyrochlore-type unit cell.

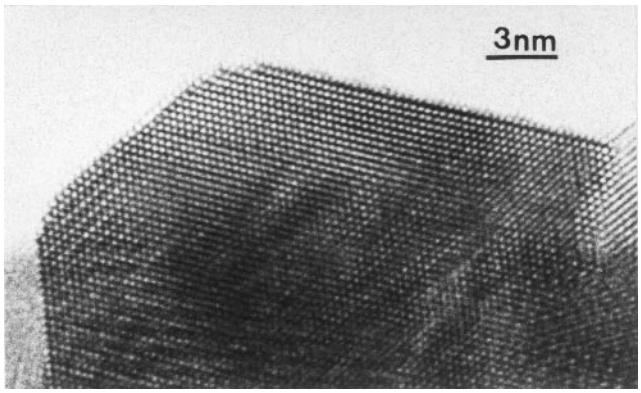

FIG. 15. Pyrochlore structure domain in a fluorite-type structure of the $Ce_{0.5}Zr_{0.5}O_{2-x}$ crystal.

$M_zR_pO_{2-x}$ ($x + y + z > 0.5$), in which M is a transition metal, especially Zr, Ti, V, Mo, W, Nb, Mn, Cu, Cr, Fe, Ni, Co, Ta, and Bi, and in which R is a rare-earth element other than Ce, Pr, or Tb. The OTC (or OSC) can be dramatically changed by the choice and concentrations of the dopants selected. For example, doping with Zr or Cu into CeO_{2-x} greatly improves its OSC(5, 15); doping Zr into a Ce–Pr–O system also improves the OSC property of $Ce_{1-x}Pr_xO_{2-x}$ (22). The modification of the content ratio of Ce, Pr, and Tb and the judicious doping of selected elements into these complex fluorite-related oxides can produce improvements in almost any application.

For hydrogen production a constant release of oxygen without peaks may oxidize the methane to hydrogen and carbon monoxide, but further absorption of oxygen from carbon monoxide causes carbon to be deposited on its surface. However, if water is supplied at the time cerium is reduced, it will reduce the water, releasing hydrogen. The release and absorption of oxygen are equally important for hydrogen production and TWC action.

3.2. Conclusions

The cyclic availability of lattice oxygen of the oxides of fluorite-type structure containing Ce, Pr, or Tb is the basis for OTC in their oxides. The OTC of these oxides is inherent in the characteristics of the fluorite structure and the variable valency of Ce, Pr, or Tb. Oxides of any of these elements having the fluorite or fluorite-related structure will have the OTC property under reducing and oxidizing conditions, without any reconstructive phase transitions. OSC and OTC data of some binary, ternary, quaternary oxides containing Ce, Pr, or Tb have been given. Using released lattice oxygen to oxidize CH_4 and taking back the oxygen from H_2O to produce hydrogen *i* is demonstrated for the quaternary oxide $Ce_{0.7}Zr_{0.25}Tb_{0.05}O_{2-x}$. The presence of OTC in fluorite-related pyrochlore structures is discussed and images of mixtures of pyrochlore-type phases are presented.

REFERENCES

1. H. C. Yao and Y. F. Yu Yao, *J. Catal.* **86,** 254 (1984).
2. S. Bernal, G. Blanco, F. J. Botana, J. M. Gatica, J. A. Perez-Omil, J. M. Pintado, and J. M. Rodriguez-Izquierdo, *J. Alloys Compd.* **207/208,** 196 (1994).
3. S. Otsuka-Yao-Matsuo, N. Izu, T. Omata, and K. Ikeda, *J. Electrochem. Soc.* **145**(4)**,** 1406 (1998).
4. D. J. M. Bevan, and J. Kordis, *J. Inorg. Nucl. Chem.* **26,** 1509 (1964).
5. P. Fornasiero, R. Di Monte, G. Ranga Rao, J. Kaspar, S. Meriani, A. Trovarelli, and M. Graziani, *J. Catal.* **151,** 168 (1995).
6. Z. L. Wang and Z. C. Kang "Functional and Smart Materials," p. 148, Plenum, New York, 1998.
7. R. E. Ferguson, E. D. Guth, and L. Eyring, *J. Am. Chem. Soc.* **76,** 3890 (1954).
8. J. M. Honig, A. F. Clifford, and P. A. Faeth, *Inorg. Chem.* **2,** 791 (1963).
9. R. G. Haire and L. Eyring, *Handb. Phys. Chem. Rare Earths* **18,** 413–505, 1994.
10. B. G. Hyde, D. J. M. Bevan, and L. Eyring, *Phil. Trans. R. Soc. A*, No. 1106, **259,** 583 (1966).
11. J. Kordis and L. Eyring, *J. Phys. Chem.* **72,** 2030 (1968).
12. J. Kordis and L. Eyring, *J. Phys. Chem.* **72,** 2044 (1968).
13. Unpublished Data.
14. Unpublished Data.
15. W. Liu and M. Flytzani-Stephanopoulos, *J. Catal.* **153,** 304 (1995).
16. K. Otsuka, Y. Wang, E. Sunada, and I. Yamanaka, *J. Catal.* **175,** 152 (1998).
17. Z. C. Kang and L. Eyring, patent pending.
18. J. Zhang, R. B. Von Dreele, and L. Eyring, *J. Solid State Chem.* **122,** 53 (1996).
19. Z. C. Kang and L. Eyring, *Aust. J. Chem.* **49,** 981 (1997).
20. unpublished data.
21. C. Lopez-Cartes, J. A. Perez-Omil, J. M. Pintado, J. J. Calvino, Z. C. Kang, and L. Eyring, *Ultramicroscopy* **80,** 19 (1999).
22. M. Yu. Sinev, G. W. Graham, L. P. Haak, and M. Shelef, *J. Mater. Res.* **11**(8), 1960 (1996).